

Large-scale reforestation can increase water yield and reduce drought risk for water-insecure regions in the Asia-Pacific

Hoong Chen Teo^{1,2}  | Srivatsan V. Raghavan^{2,3,4}  | Xiaogang He^{2,5}  |
 Zhenzhong Zeng⁶  | Yanyan Cheng⁷  | Xiangzhong Luo^{2,4}  | Alex M. Lechner⁸  |
 Matthew J. Ashfold⁹  | Aakash Lamba^{1,2}  | Rachakonda Sreekar^{1,2}  |
 Qiming Zheng^{1,2}  | Anping Chen¹⁰  | Lian Pin Koh^{1,2,3} 

¹Department of Biological Sciences, National University of Singapore, Singapore, Singapore

²Centre for Nature-based Climate Solutions, National University of Singapore, Singapore, Singapore

³Tropical Marine Science Institute, National University of Singapore, Singapore, Singapore

⁴Department of Geography, National University of Singapore, Singapore, Singapore

⁵Department of Civil and Environmental Engineering, National University of Singapore, Singapore, Singapore

⁶School of Environmental Science and Engineering, Southern University of Science and Technology, Shenzhen, China

⁷Department of Industrial Systems Engineering & Management, National University of Singapore, Singapore, Singapore

⁸Urban Transformations Hub, Monash University Indonesia, Tangerang Selatan, Indonesia

⁹School of Environmental and Geographical Sciences, University of Nottingham Malaysia, Semenyih, Malaysia

¹⁰Graduate Degree Program in Ecology, Department of Biology, Colorado State University, Fort Collins, Colorado, USA

Correspondence

Hoong Chen Teo and Lian Pin Koh,
 Department of Biological Sciences,
 National University of Singapore,
 Singapore, Singapore.
 Email: hcteo@u.nus.edu and lianpinkoh@nus.edu.sg

Funding information

Ministry of Education Singapore, Grant/
 Award Number: A-0009297-01-00, A-
 8000190-00-00 and R-109-000-272-133;
 National Research Foundation Singapore,
 Grant/Award Number: NRF-RSS2019-007

Abstract

Large-scale reforestation can potentially bring both benefits and risks to the water cycle, which needs to be better quantified under future climates to inform reforestation decisions. We identified 477 water-insecure basins worldwide accounting for 44.6% (380.2 Mha) of the global reforestation potential. As many of these basins are in the Asia-Pacific, we used regional coupled land-climate modeling for the period 2041–2070 to reveal that reforestation increases evapotranspiration and precipitation for most water-insecure regions over the Asia-Pacific. This resulted in a statistically significant increase in water yield ($p < .05$) for the Loess Plateau–North China Plain, Yangtze Plain, Southeast China, and Irrawaddy regions. Precipitation feedback was influenced by the degree of initial moisture limitation affecting soil moisture response and thus evapotranspiration, as well as precipitation advection from other reforested regions and moisture transport away from the local region. Reforestation also reduces the probability of extremely dry months in most of the water-insecure regions. However, some regions experience nonsignificant declines in net water yield due to heightened evapotranspiration outstripping increases in precipitation, or declines in soil moisture and advected precipitation.

KEY WORDS

forest–water nexus, natural climate solutions, nature-based solutions, precipitation, socio-ecological systems, water balance, water risk, water stress

1 | INTRODUCTION

The growing climate crisis has attracted increasing attention to the potential of nature-based solutions for mitigating anthropogenic climate change, with reforestation emerging as one of the most attractive solutions (Fargione et al., 2008; Koh et al., 2021; Teo, Zeng, et al., 2021). Since reforestation only occurs in areas considered biophysically suitable for forest biomes, it is commonly perceived as an ecologically low-risk “no regrets” solution, potentially offsetting one-third of the global anthropogenic carbon emissions annually if fully realized globally (Griscom et al., 2017) while delivering a slew of co-benefits, such as biodiversity conservation, soil protection, hydrological benefits, and other ecosystem services (Cheng, Huang, et al., 2022; Cui et al., 2021; Kemppinen et al., 2020; Mori et al., 2021; Sarira et al., 2022).

While reforestation can deliver many potential socio-ecological benefits, it also has far more complex impacts on the regional water balance. Forests may be either consumers or suppliers of water-consuming water through evapotranspiration, while also potentially stimulating more precipitation by intensifying moisture recycling (Bennett & Barton, 2018; Ellison et al., 2012). The net effect of both demand and supply-side processes is reflected in the water yield (defined as precipitation minus evapotranspiration hereafter), which is the net water supply available for ecosystem processes such as groundwater recharge, and human uses such as agriculture and domestic consumption. Although many studies have documented increases in water yield from reforestation (Filoso et al., 2017; Meier et al., 2021; Zhang et al., 2022), other studies have also shown reforestation projects to reduce water yield, especially in water-stressed or semi-arid regions (Feng et al., 2016; Trimble et al., 1987; Yao et al., 2015). There is a need for a comprehensive assessment of the potential benefits and risks of reforestation to the water cycle over broad geographical regions, particularly for basins facing water insecurity under future climate conditions.

The development of evapotranspiration models has enabled the estimation of potential changes in evapotranspiration from reforestation (Hamon, 1961; Lu et al., 2005). However, the net effect on water yield taking into account both demand- and supply-side interactions requires coupled land-atmosphere modeling. These models consider locally controlled biogeophysical processes such as soil moisture responses (Koster et al., 2004; Seneviratne et al., 2010), and larger scale atmospheric interactions such as advective moisture transport (Abiodun et al., 2012; Cerasoli et al., 2021), which can thus produce spatially explicit and policy-relevant projections on the reforestation-water nexus. Moreover, many coupled land-atmosphere models have the ability to model changes in stomatal conductance and hence evapotranspiration due to rising CO₂ levels in a future climate (Oleson et al., 2013; Sellers et al., 1996), reducing a major uncertainty faced by offline empirical calculations where stomatal conductance may not be modeled (Hoek van Dijke et al., 2022).

Focusing on potentially reforestable lands and using river basins as the unit of analysis, here we aimed to address two main questions

regarding possible hydrological impacts from reforestation: to (1) identify projected water-insecure basins where reforestation may significantly affect water yield, and (2) quantify what those impacts might be under future climate conditions. Firstly, using global climate projection datasets, we identified projected water-insecure basins worldwide by modeling and mapping (a) water-stressed basins, (b) drylands, and (c) the potential decline in water yield due to increased evapotranspiration from reforestation (demand-side). Secondly, we used high-resolution regional coupled land-climate models to evaluate the effects of reforestation on evapotranspiration, precipitation and the water cycle, accounting for both demand and supply-side interactions across the Asia-Pacific, where many densely populated basins face water insecurity issues.

2 | METHODS

2.1 | Identifying projected water-insecure basins sensitive to water yield changes globally

Reforestation potential areas are land with the biophysical potential for forest cover (excluding boreal, grass, and savannah biomes), minus existing forest and areas socially incompatible with returning to forests, such as cropland and densely populated rural areas. Using Griscom et al.'s (2017) widely used global reforestation potential map produced at 1-km resolution according to this definition, and level 5 HydroBASINS to represent hydrological basins (Lehner & Grill, 2013), we first mapped basins where the potentially reforestable area is larger than 10%. Our reforestation scenario assumes that the reforestation potential is entirely fulfilled at present, giving around two decades (to 2040) for the land cover to be restored to forest. Using this scenario, we mapped basins worldwide that could potentially face water insecurity issues from reforestation, based on meeting at least one of three criteria below at any decade during our simulation duration (2040s, 2050s, and 2060s).

1. Water-stressed basins. Water stress is measured by the withdrawals-to-availability ratio or relative water demand, which is the ratio of the demand for water by human society divided by available water. We consider any basin where relative water demand (averaged over all pixels within the basin) exceeds 0.2, to be water stressed, in line with commonly used definitions (Alkon et al., 2019; Luck et al., 2015; Satoh et al., 2017). For each decadal period (2040s, 2050s, 2060s), we took the multimodel ensemble mean of water stress for five RCP4.5 CMIP5 bias-corrected GCM projections (GFDL-ESM2M, HadGEM2, IPSL-CM5A-LR, MIROC-ESM, and NorESM1-M), derived from the 0.5° resolution Water Futures and Solutions (WFaS) dataset (Satoh et al., 2017).
2. Dryland basins, defined by the mean basin Aridity Index (AI) < 0.65. AI is precipitation (P) divided by potential evapotranspiration (PET) and reflects the degree of long-term climatic water deficits. We calculated AI for the 2040s, 2050s, and 2060s. P and daily mean air

temperature (T) were derived from the multimodel ensemble mean of 31 RCP4.5 CMIP5 GCM projections extracted from Navarro-Racines et al.'s (2020) 30 arc-sec resolution bias-corrected high-resolution downscaled dataset. Using P , T , and daytime length, PET was calculated using Hamon's equation (Hamon, 1961):

$$\text{PET} = k \times 0.1641 \times L_d \times \rho_s \quad (1)$$

$$\rho_s = 216.7 \times \frac{e_s}{T + 273.3} \quad (2)$$

$$e_s = 6.108 e^{\frac{17.26939 T}{T+237.3}} \quad (3)$$

where PET is potential evapotranspiration (mm day^{-1}); k is a proportionality coefficient, set at 1.2 for this study; L_d is the daytime length, which is the time from sunrise to sunset in multiples of 12 h; ρ_s is the saturated vapor density (g m^{-3}) at T ($^\circ\text{C}$); and e_s is the saturated vapor pressure (mb) at the given T .

Hamon's equation was selected as the variables required were available from Navarro-Racines et al.'s (2020) high-resolution projections for a large number of CMIP5 GCMs, while other equations often require additional variables available only at coarser resolution and for fewer GCMs. Hamon's equation is one of the more widely used PET estimation equations and has been noted to perform well in various biomes (Lu et al., 2005; Paparrizos et al., 2016).

3. Water yield ($Q = P - \text{ET}$) projected to decline by >5% due to fulfilling Griscom et al.'s (2017) reforestation potential (Yao et al., 2015). Water yield (Q) decline was modeled as demand-side only (assuming no changes to P , and models forest consumption of water as an increase in evapotranspiration, ET). For each decadal period (2040s–2060s), a baseline scenario was created using 0.05° resolution land cover fraction data derived from the multimodel ensemble mean of five downscaled RCP4.5–SSP2 CMIP5 GCMs (GFDL-ESM2M, HadGEM2-ES, IPSL-CM5A-LR, MIROC5, and NorESM1-M) (Chen et al., 2020), and a reforestation scenario was created by modifying the baseline scenario to fulfill Griscom et al.'s (2017) reforestation potential in its entirety. Climatic data were the RCP4.5 31-model ensemble means derived from Navarro-Racines et al. (2020), resampled to 0.05° resolution. PET was calculated from Equations (1–3) above using the same methods and source data. ET was calculated using equations derived from Zhang et al. (2001), simplified as follows:

$$\text{ET} = \sum_{i=k}^n \left(l_i \times P \times \left[1 + \frac{w_i \times \text{PET}}{P} \right] \left[1 + \frac{w_i \times \text{PET}}{P} + \frac{P}{\text{PET}} \right]^{-1} \right) \quad (4)$$

where ET is evapotranspiration (mm day^{-1}); PET is potential evapotranspiration (mm day^{-1}); P is precipitation (mm day^{-1}); l_i is the land

cover fraction for land cover i ; w_i is the plant-available water coefficient for land cover i , defined in this study as $w = 0.5$ (crop/grass), 1.0 (shrub), 2.0 (forest) as per Zhang et al. (2001).

We further validated our method of calculating ET and PET from Hamon's equations and Zhang et al. (2001) for the historical period of 2010–2019, against the MODIS Terra (MOD16A2.006) product which is derived from MODIS Terra remote sensing information and processed with the Penman–Monteith equation. The Penman–Monteith equation is more complex and is well regarded given its use as the default by MODIS, the FAO, and others (Cai et al., 2007; Schymanski & Or, 2017). Our ET and PET derived from Hamon's equation were highly correlated with the MODIS Terra product with $r = .81$ ($p < .01$) for ET and $r = .84$ ($p < .01$) for PET, across all level 5 HydroBASINS globally ($n = 4338$) (details in Figure S1). We thus consider Hamon's equation as suitably robust for our application.

2.2 | Regional climate modeling of water-insecure regions

In order to understand the possible climatic and hydrologic feedbacks of reforestation on water yield, taking into account the supply-side (changes in moisture recycling and precipitation) in addition to demand-side (increase in evapotranspiration), we ran a coupled land–atmosphere regional climate model, the International Centre for Theoretical Physics (ICTP) Regional Climate Model version 4.7, coupled to the Common Land Model version 4.5 (RegCM4.7-CLM4.5), to dynamically downscale RCP4.5 GCM outputs from 2040 to 2070 under two scenarios: (a) a baseline scenario with default land cover and (b) a reforestation scenario with Griscom et al.'s (2017) reforestation potential fully fulfilled across the entire domain. RegCM4.7 performs radiative transfer calculations for the atmosphere, simulates planetary boundary layer processes including cumulus convection, and contains a resolved scale precipitation scheme. CLM4.5 represents land–atmosphere exchanges of energy, momentum, water, and carbon, within a subgrid of different land cover and vegetation fractions for each grid cell, calculating biogeophysical processes for each and returning them to the atmospheric model of RegCM4.7. Notably, CLM4.5 models the effect of stomatal conductance on net leaf photosynthesis, scaled by relative humidity and CO_2 concentration at the leaf surface, using parameterizations from Sellers et al. (1996). The model is initiated by the user with land cover and parameterization schemes, as well as initial and boundary climatic conditions from observations, reanalysis or coarser GCM outputs. Atmospheric variables are output from RegCM4.7, while land surface variables are output from CLM4.5.

RCP4.5 was selected as it is the intermediate scenario representing the most probable future climatic conditions. The CLM4.5 default dynamic land cover dataset for the future (Oleson et al., 2013) is based on the Land Use Harmonization A version 1 (LUHa.v1) product (Hurt et al., 2011), and represents vegetation with 16 plant functional types (PFT) (Table S1). For each grid cell, the reforestation potential was distributed among the different forested PFTs at the same proportion as the baseline land cover.

The climate simulations were conducted for four Coordinated Regional Climate Downscaling Experiment (CORDEX) domains across the Asia-Pacific: Australasia, East Asia, South Asia and Southeast Asia (Figure S2), at 40-km horizontal resolution, a resolution at which RegCM has been noted to perform well at Karadan et al. (2021). Eighteen vertical levels were used from the surface up to 50 hPa, top of the atmosphere (TOA). Lambert conformal projection was used for each domain. The model was simulated using the hydrostatic dynamical core with a time step of 50 s, surface at 10 min, solar radiation at 30 min, and absorption–emission at 18 h. The following parameterization schemes were used: Holtslag et al. (1990) counter gradient for the planetary boundary layer, Emanuel (1991) cumulus convection over land and ocean, Pal et al.'s (2000) subgrid explicit moisture and cloud scheme (SUBEX) for moist processes, and Zeng et al. (1998) for ocean flux.

Historical validation for 1991–2000 (the first year 1990 discarded as spin-up) was first performed on the ERA5 monthly reanalysis dataset (Hersbach et al., 2019) and indicated good results at the region level with Pearson's $r = .74$ ($p < .01$) for P and $r = .87$ ($p < .01$) for ET, as well as a generally good representation of seasonality (Figures S3–S5). We used a generous period of 1 year as spin-up for model stabilization, as other RegCM studies have found spin-ups of 1–2 months sufficient (Kumar & Dimri, 2020; Maity et al., 2021); we noted no issues with model stability after discarding the first year spin-up. Next, we used five RCP4.5 CMIP5 GCMs (HadGEM2, MPI-ESM-MR, NorESM1-M, GFDL-ESM2M, and CSIRO-MK36) as initial and boundary conditions to force our baseline and reforestation scenarios for 2041–2070 (the first year 2040 discarded as spin-up). The median of five GCM-forced RegCM outputs was taken for each pixel to generate a multimodel median. Results were reported for 15 water-insecure regions which were aggregated from the water-insecure basins (Figure S5), to form a larger contiguous region more appropriate for the RegCM resolutions. The smallest region, Taiwan, comprised 17 pixels. Within the domains, basins too small and distant from other basins to form sufficiently large contiguous regions were not evaluated.

To further confirm that there were no issues with transpiration/evapotranspiration (T/ET) partitioning in our results (Lawrence et al., 2007; Wang et al., 2014), we examined decadal mean T/ET ratios for the study duration across the water-insecure regions studied (Figure S6). As expected, the T/ET ratio increases with increasing forest coverage (Pearson's $r = .39$, $p < .01$). Moreover, given the modeled increase in evapotranspiration due to reforestation from our results, we find the T/ET partitioning in RegCM4.7-CLM4.5 satisfactory.

Extreme value analysis of precipitation in the wettest and driest months in each water-insecure region was conducted using an r -largest/smallest generalized extreme values (GEVr) model with annual blocks, using the R package "eva" (Bader & Yan, 2020). The GEVr approach uses more information from the data than a block maxima/minima approach, thereby reducing potential biases. The entropy difference and multiplier bootstrap specification tests were used to evaluate the best r values between 1 and 4 for each

water-insecure region (Bader et al., 2016). The best r was selected for each region using the lowest ForwardStop values statistically significant at $p < .05$, and the mean was taken for all regions. Rounded to the nearest integer, the best r -largest order statistic was 4 (i.e., 4 wettest months) and the best r -smallest order statistic was 3 (i.e., 3 driest months). GEVr models were constructed using these r values, and 50-year return levels were computed using the delta method.

To understand the effects of reforestation on precipitation recycling, we calculate the recycling ratio for both baseline and reforestation scenarios at pixel level. Following Brubaker et al. (1993), we consider precipitation and evaporation over a land region as each comprising advected and locally generated components. Advected moisture decreases linearly as air moves across the region, while locally evaporated moisture content increases linearly; as the atmosphere is assumed to be fully mixed, precipitation from advected and local moisture sources is proportionate to the ratio of advected to local moisture present in the air column. We derived the fraction of precipitation due to local terrestrial origin, or precipitation recycling ratio (R), within 1000 km windows, as:

$$R = \left[1 + 2 \frac{\sum_{i=1}^n (w_i u_i)}{ET \times l} \right]^{-1}$$

$$w_i = \frac{q_i \times p_i}{g}$$

where the rate of water vapor flux into the local region $w_i u_i$ ($\text{kg m}^{-1} \text{s}^{-1}$) for each vertical level i is the product of precipitable water w_i (kg m^{-2}) and velocity u_i (m s^{-1}); ET is local evapotranspiration (mm s^{-1}); l is the length scale traversed by the air parcel; q_i (kg kg^{-1}) is the specific humidity at vertical level i ; p_i is the pressure at vertical level i (Pa); and g is the gravitational constant of 9.8 m s^{-2} .

3 | IDENTIFYING PROJECTED WATER-INSECURE BASINS IN REFORESTATION POTENTIAL AREAS

Among the basins with substantial reforestation potential ($> 10\%$ of the basin's land area), we identified 165 water-stressed basins, 270 dryland basins, and 275 basins with a potential water yield decline of $>5\%$ due to increased evapotranspiration from reforestation (modeled demand-side only; see Methods). Respectively, these three types of basins accounted for 15.4% (131.4 Mha), 22.6% (192.2 Mha), and 29.3% (250.0 Mha) of global reforestation potential. Combined, there are a total of 477 unique basins meeting at least one of the three criteria for water-insecure basins as defined above, accounting for 44.6% (380.2 Mha) of the global reforestation potential (Figure 1). These are the water-insecure basins where reforestation can be the most beneficial or detrimental to water yield. In particular, there are 43 unique basins meeting all the three criteria, accounting for 4.7% (40.0 Mha) of the global reforestation potential.

Water-insecure basins can be found across all nonpolar latitudes and continents (Figure 1b,f), with major hotspots in China, India, Australia, the Mediterranean, Mexico, and Brazil. Notably, the subtropical latitudes have the highest proportion of water-insecure reforestation potential (54.3% of subtropical total). Tropical latitudes have the lowest proportion of water-insecure reforestation

potential (39.6% of tropical total), with much of this found toward the seasonal tropics rather than toward the equator. Globally, there are 1.91 billion people as of 2020 (WorldPop, 2021) living in these water-insecure basins with substantial reforestation potential, of which 1.35 billion (69%) are in the Asia-Pacific region. As such, we focus on the Asia-Pacific for our subsequent analyses.

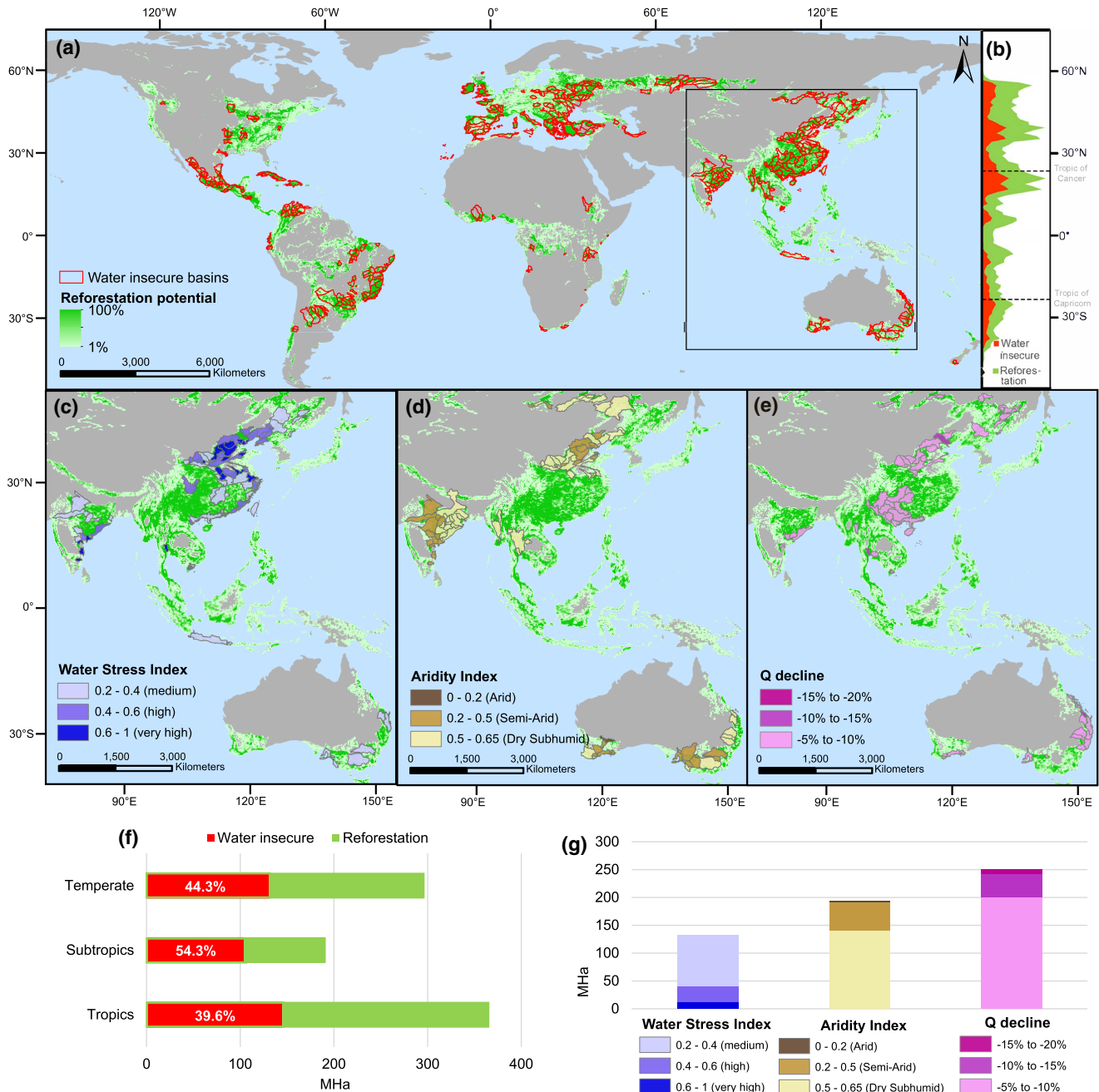


FIGURE 1 Global water-insecure basins over reforestation potential area. (a) There are 477 water-insecure basins worldwide with >10% of land reforestable, accounting for 44.6% (380.2 Mha) of the global reforestation potential. These are basins meeting one of three criteria in any decade during the 2040s, 2050s, and 2060s: Water stress index (WSI) > 0.2, aridity index (AI) < 0.65, or projected water yield (Q) decline from reforestation (without supply-side feedbacks) > 5%. (b) Latitudinal distribution of reforestation potential in water-insecure basins as a proportion of total reforestation potential. (c–e) Basins in the Asia-Pacific meeting the criteria: WSI > 0.2, where higher (darker) WSI indicates higher water stress (c); AI < 0.65, where lower (darker) AI indicates higher aridity (d); Q decline of >5% without supply-side feedbacks, where lower (darker) indicates higher magnitude of Q decline (e). (f) Proportion of total reforestation potential in water-insecure basins per latitudinal zone. (g) Amount of reforestation potential in basins meeting each of the three criteria above.

4 | MODELING THE HYDROLOGICAL IMPACTS OF REFORESTATION ON WATER-INSECURE REGIONS

4.1 | Main findings

Regional climate modeling was conducted for 2041–2070 using a baseline (default land cover) and reforestation scenario, over four domains across the Asia-Pacific (Australasia, East Asia, South Asia, and Southeast Asia) at a 40-km horizontal resolution for RCP4.5 climate settings (see Methods for details). Under the reforestation scenario, the reforestation potential identified by Griscom et al. (2017) would be entirely fulfilled across the entire domain (i.e., reforestable land cover had become forest by 2040), and results were reported for 15 water-insecure regions which were aggregated from the water-insecure basins in the Asia-Pacific.

Our results confirm the strong effects of reforestation on the water cycle and affirm the notion that forests increase evapotranspiration (Filoso et al., 2017; Li et al., 2018), with this serving as the main initial driver for further climatic changes at local and regional scales. An increase in evapotranspiration was shown in 13 of 15 regions, which was statistically significant ($p < .05$, paired student's *t*-test in this study) in eight regions; reforestation potential in these eight regions ranged from 24.2% to 33.3% of their total land areas (Table 1; Figure 2). Supporting the supply-side conception of forests as positive contributors to precipitation and thus the water cycle, an increase in precipitation was shown in 11 of 15 regions following reforestation, which was statistically significant in seven regions (Table 1). The overall effect of reforestation on water yield was beneficial for some regions. An increase in water yield was shown in 7 of 15 regions, which was statistically significant in four regions—Loess Plateau–North China Plain ($11.4 \pm 11.8\%$), Yangtze Plain ($16.9 \pm 3.3\%$), Southeast China ($17.6 \pm 6.4\%$), and Irrawaddy ($84.9 \pm 24.7\%$) (Table 1). None of the declines in water yield were statistically significant.

Reforestation was broadly shown to reduce the probability of extremely dry months (Table 2), especially in regions with an increase in total annual precipitation. A decline in extreme dry events (lowest monthly precipitation occurring at a 50-year return interval) was observed in 9 of 15 regions, of which six regions had an increase in annual total precipitation. The effect of reforestation in moderating extreme wet months was equivocal. A decline in extreme wet events (highest monthly precipitation occurring at a 50-year return interval) was observed in 7 of 15 regions, of which four regions had an increase in total annual precipitation.

4.2 | Monsoon interactions with soil moisture and advection

To further understand possible mechanisms behind the divergent responses of different regions, we extracted soil moisture and calculated the precipitation recycling ratio (fraction of precipitation

from local terrestrial origin, rather than advected origin). Previous studies have highlighted the key role of soil moisture responses in influencing the local evapotranspiration response following reforestation (Koster et al., 2003; Seneviratne et al., 2010). Forests increase root depth compared to other vegetation types, facilitating more soil moisture mining and storage (Cheng et al., 2018; Cheng, Leung, et al., 2022). Generally, evaporation is thought to be more sensitive to soil moisture in the transition zones between wet and dry climates, which are dry enough for evaporation to be moisture limited, yet not too dry that the absolute value and variation in soil moisture are too little to affect evaporation (Koster et al., 2004). We noted a significant increase in soil moisture in 9 of 15 regions following reforestation (Table 3a), corresponding closely to the regions with increased evapotranspiration (Table 1). These regions were neither too wet nor too dry, with baseline soil moisture ranging between $0.260 \text{ m}^3 \text{ m}^{-3}$ and $0.277 \text{ m}^3 \text{ m}^{-3}$, and baseline mean annual precipitation ranging between 336.1 m y^{-1} and 1101.0 m y^{-1} . Koster et al.'s (2004) analysis of regions with strong soil moisture–evapotranspiration coupling in general circulation models highlighted very strong coupling over East-Central India and strong coupling over North China, with no signal over Australia. This is in line with our results from regional climate modeling.

Given that advected precipitation accounts for the majority of total precipitation, as confirmed by our study as well as other precipitation recycling studies, for example (Holgate et al., 2020; Pathak et al., 2014), atmospheric moisture transport patterns strongly influence precipitation responses from reforestation, especially at regional scales. We found that reforestation did not significantly change the large-scale circulations of the East Asian and Indian summer and winter monsoons compared to the RCP4.5 baseline, with the prevailing wind vectors at 850 hPa for the reforestation experiments following the same pattern as the baseline experiments (depicted in Figures 3f and 4f). As such, additional evapotranspired moisture from reforestation was advected downwind following the same large-scale monsoon circulations, with varying effects on the upwind and downwind areas, especially depending on their degree of moisture limitation.

The Indian summer monsoon contains both an Arabian Sea and Bay of Bengal branch, both of which travel overland across East-Central India; coastal areas receive large amounts of oceanic-origin moisture with further moisture propagation to drier inland areas having a larger continental precipitation recycling component (Gupta et al., 2005; Sengupta & Sarkar, 2006). Moreover, East-Central India is relatively dry, hosting semiarid and dry subhumid climates (Figure 1d), and has been noted to have strong soil moisture–evapotranspiration coupling (Koster et al., 2004). Reforestation thus has very significant effects on East-Central India during summer, with a $37.9 \pm 34.1\%$ increase in locally generated summer precipitation leading to a $16.9 \pm 11.6\%$ increase in total summer precipitation (Table 4b). Soil moisture increases significantly, with this increase persisting throughout the winter dry season (Table 4a,b). In winter, northern and central India experience extratropical cyclonic activity in the form of “western

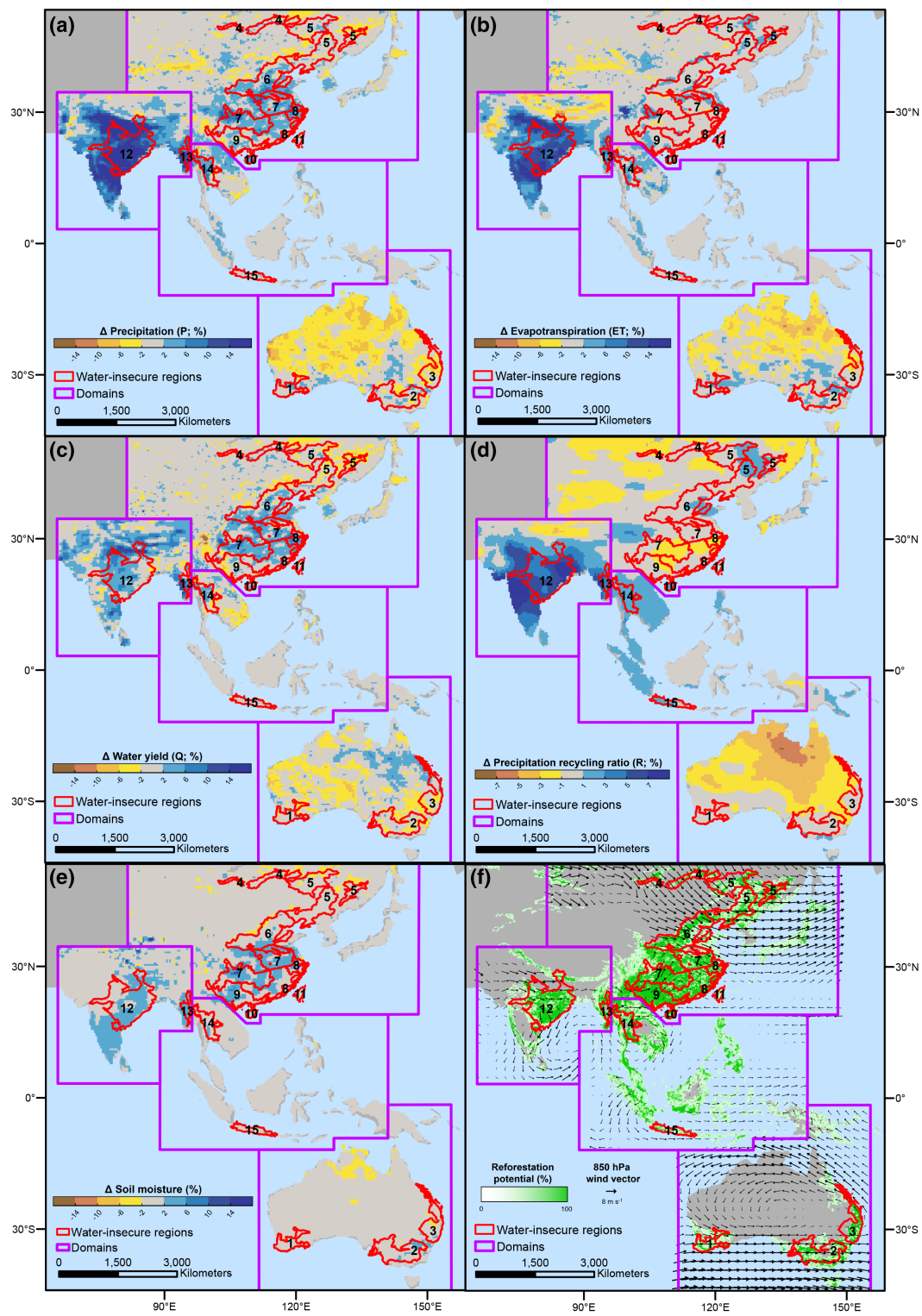


FIGURE 2 Mean percentage change in annual precipitation (P) (a), evapotranspiration (ET) (b), water yield (Q) (c), the precipitation recycling ratio (R) (d), and soil moisture (e) between 2041 and 2070 in the Asia-Pacific, due to fully realizing the domain reforestation potential by 2040 (f). Annual baseline wind vectors at 850 hPa are shown in (f). Regional climate modeling was separately conducted for four CORDEX domains (Australasia, East Asia, South Asia, and Southeast Asia); domain boundaries indicated in this figure are the boundaries used for reporting results.

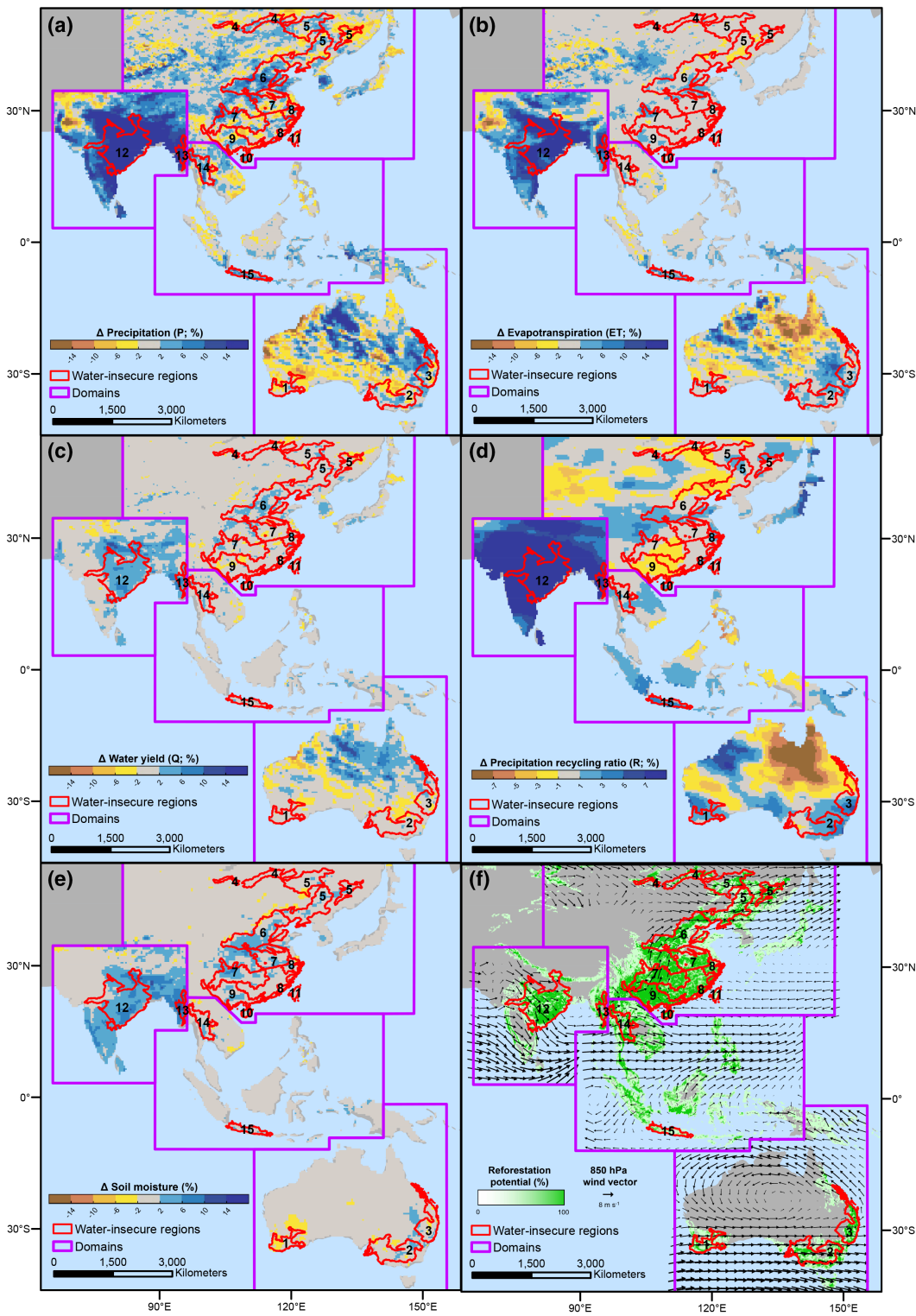


FIGURE 3 Mean percentage change in summer (JJA) precipitation (P) (a), evapotranspiration (ET) (b), water yield (Q) (c), the precipitation recycling ratio (R) (d), and soil moisture (e) between 2041 and 2070 in the Asia-Pacific, due to fully realizing the domain reforestation potential by 2040 (f). Baseline summer wind vectors at 850 hPa are shown in (f). Regional climate modeling was separately conducted for four CORDEX domains (Australasia, East Asia, South Asia, and Southeast Asia); domain boundaries indicated in this figure are the boundaries used for reporting results.

TABLE 1 Percentage change in water yield (Q), precipitation (P), and evapotranspiration (ET) between 2041 and 2070 in water-insecure regions of the Asia-Pacific, due to fully realizing the domain reforestation potential by 2040. Each region^a was assessed to be “beneficial”/“caution advised”^b with a confidence level (h.c. for high confidence, m.c. for medium confidence, and l.c. for low confidence), or neutral. Figures reported are $M \pm SD$

No.	Domain	Region	Major rivers	% area reforestable	ΔQ (%)	ΔP (%)	ΔET (%)	Reforestation-water assessment
1	Australasia	Southwest Australia	Blackwood, Swan	19.0	-1.2 ± 5.4	0.4 ± 2.8	0.5 ± 4.6	Caution advised (l.c.)
2		Murray-Darling	Murray, Darling	15.4	-11.5 ± 17.1	0.0 ± 2.7	1.3 ± 4.0	Caution advised (l.c.)
3		East Australia	Brisbane, Logan, Murray	26.5	-0.4 ± 6.9	-2.0* ± 2.2	-1.7 ± 3.1	Caution advised (m.c.)
4	East Asia	Siberia	Selenga, Shilka	16.4	-1.6 ± 5.3	-0.0 ± 1.3	0.3 ± 2.6	Caution advised (l.c.)
5		Manchurian Plain	Songhua, Liao, Amur	18.4	-3.1 ± 3	-0.4 ± 1.1	0.6* ± 1.8	Caution advised (m.c.)
6		Loess Plateau-North China Plain	Yellow, Hai	26.3	11.4* ± 11.8	2.6* ± 2.6	0.6* ± 2.1	Beneficial (h.c.)
7		Yangtze Plain	Yangtze, Huai	33.3	16.9* ± 3.3	3.6* ± 1.0	0.3 ± 0.9	Beneficial (h.c.)
8		Southeast China	Qiantang, Jiulong	24.2	17.6* ± 6.4	4.0* ± 1.7	-0.0 ± 0.8	Beneficial (h.c.)
9		Pearl	Pearl, Red	44.4	-3.9 ± 7.3	0.3 ± 1.4	1.0* ± 1.1	Caution advised (l.c.)
10		Hainan	Changhua, Wanquan	41.3	23.0 ± 41.3	2.9* ± 2.0	2.1* ± 2.2	Beneficial (m.c.)
11		Taiwan	Tamsui, Kaoping	12.8	-1.0 ± 5.5	-0.5 ± 3.1	0.1 ± 0.7	Neutral ^c
12	South Asia	East-Central India	Ganges, Godavari	24.8	7.3 ± 8.7	12.9* ± 4.1	10.9* ± 6.2	Beneficial (m.c.)
13		Irrawaddy	Irrawaddy	29.8	84.9* ± 24.7	10.8* ± 2.3	5.6* ± 1.7	Beneficial (h.c.)
14	Southeast Asia	Chao Phraya	Chao Phraya, Salween	27.8	17.0 ± 25.5	3.2* ± 1.9	2.3* ± 2.6	Beneficial (m.c.)
15		Java-Bali	Bengawan Solo, Citarum	11.6	-99.7 ± 657.8	0.6 ± 1.8	0.7* ± 2.4	Caution advised (l.c.)

Note: Bold and * indicate statistical significance ($p < .05$, paired student's t-test); italics indicates decrease.

^aWater-insecure regions are aggregated from adjacent water-insecure basins (Figure 1); note that region names and major rivers listed denote the general area covered by these water-insecure basins and do not necessarily include the entire region/river basins named.

^bOur assessment on whether reforestation may be beneficial or risky for each water-insecure region used the following criteria: (1) reforestation is considered “Beneficial” to the water cycle if it causes an increase in Q , and “Caution Advised” if it causes a decrease in Q ; our assessment is (2) high confidence (h.c.) if Q change is statistically significant; (3) medium confidence (m.c.) if Q not statistically significant but P is statistically significant, and Q and P move in the same direction; (4) low confidence (l.c.) for all other results.

^cTaiwan was assessed to be “Neutral” due to the very small magnitude and % of Q change relative to the large and positive Q ($\text{mm } \text{yr}^{-1}$) values.

TABLE 2 Change in estimated highest and lowest monthly P occurring at 50-year return intervals between 2041 and 2070 in water-insecure regions of the Asia-Pacific, due to fully realizing the domain reforestation potential by 2040. Figures reported are $M \pm SD$

No.	Domain	Region	ΔP (%)	% Δ highest monthly P at 50-year return interval	% Δ lowest monthly P at 50-year return interval	Description
1	Australasia	Southwest Australia	0.4 \pm 2.8	-3.5 \pm 24.9	-4.1 \pm 32.4	Less extreme wet, more extreme dry
2		Murray-Darling	0.0 \pm 2.7	2.0 \pm 25.9	-7.8 \pm 21.6	More extreme wet and dry
3		East Australia	-2.0* \pm 2.2	-11.3 \pm 32.0	9.6 \pm 32.3	Less extreme wet and dry
4	East Asia	Siberia	-0.0 \pm 1.3	-3.9 \pm 18.9	-0.5 \pm 14.2	Less extreme wet, more extreme dry
5		Manchurian Plain	-0.4 \pm 1.1	3.6 \pm 17.3	2.1 \pm 24	More extreme wet, less extreme dry
6		Loess Plateau–North China Plain	2.6* \pm 2.6	1.0 \pm 17.0	-3.2 \pm 43.4	More extreme wet and dry
7		Yangtze Plain	3.6* \pm 1.0	-7.3 \pm 23.5	4.6 \pm 29.2	Less extreme wet and dry
8		Southeast China	4.0* \pm 1.7	5.7 \pm 19.2	0.1 \pm 41.4	More extreme wet, less extreme dry
9		Pearl	0.3 \pm 1.4	-1.9 \pm 23.1	10.1 \pm 38.1	Less extreme wet and dry
10		Hainan	2.9* \pm 2.0	8.6 \pm 25.7	-4.2 \pm 26.6	More extreme wet and dry
11		Taiwan	-0.5 \pm 3.1	-9.0 \pm 26.6	5.9 \pm 29.8	Less extreme wet and dry
12	South Asia	East-Central India	12.9* \pm 4.1	21.8* \pm 40.4	0.8 \pm 31.9	More extreme wet* , less extreme dry
13		Irrawaddy	10.8* \pm 2.3	11.7 \pm 27.7	-43.4* \pm 100.4	More extreme wet and dry*
14	Southeast Asia	Chao Phraya	3.2* \pm 1.9	-1.2 \pm 27.1	0.9 \pm 41.6	Less extreme wet and dry
15		Java-Bali	0.6 \pm 1.8	3.4 \pm 20.8	1.3 \pm 24.2	More extreme wet and dry

Note: Bold and * indicate statistical significance ($p < .05$, paired student's t-test); italics indicates less desirable directional change—increase for highest monthly P (wetter wet), and decrease for lowest monthly P (drier dry).

TABLE 3 Changes in annual soil moisture (a), precipitation (P), local precipitation recycling ratio (R), and P from local and advected origin (b) compared with other key variables between 2041 and 2070 in water-insecure regions of the Asia-Pacific, due to fully realizing the domain reforestation potential by 2040. Figures reported are $M \pm SD$

No.	Domain	Region	(a) Annual soil moisture			(b) Annual precipitation recycling						
			% area reforestable	Baseline mean P (mm y^{-1})	Baseline mean soil moisture ($\text{m}^3 \text{m}^{-3}$)	Δ soil moisture (%)	ΔP (%)	ΔR (%)	Δ local P (mm y^{-1})	$\% \Delta$ local P	Δ advected P (mm y^{-1})	$\% \Delta$ advected P
1	Australasia	Southwest Australia	19.0	205.2 \pm 30.0	0.089 \pm 0.004	-0.17 \pm 1.65	0.4 \pm 2.8	0.3 \pm 7.6	-0.0 \pm 1.7	-0.2 \pm 9.6	0.8 \pm 4.2	0.4 \pm 2.3
2		Murray-Darling	15.4	295.1 \pm 38.5	0.105 \pm 0.006	0.81 \pm 2.20	0.0 \pm 2.7	-0.3 \pm 6.0	0.0 \pm 3.3	0.0 \pm 7.9	0.0 \pm 5.8	0.0 \pm 2.3
3		East Australia	26.5	528.6 \pm 61.0	0.119 \pm 0.007	-0.32 \pm 2.32	-2.0* \pm 2.2	-0.8 \pm 4.3	-3.2 \pm 7.7	-3.1 \pm 7.3	-7.3 \pm 7.2	-1.7 \pm 1.7
4	East Asia	Siberia	16.4	516.1 \pm 34.7	0.274 \pm 0.011	-0.37 \pm 1.49	-0.0 \pm 1.3	-0.4 \pm 3.3	-0.8 \pm 8.1	-0.4 \pm 4.1	0.7 \pm 3.9	0.2 \pm 1.2
5		Manchurian Plain	18.4	715.1 \pm 37.3	0.273 \pm 0.006	-0.06 \pm 0.88	-0.4 \pm 1.1	0.5 \pm 2.4	-1.2 \pm 8.2	-0.5 \pm 3.4	-1.3 \pm 4.3	-0.3 \pm 0.9
6		Loess Plateau–North China Plain	26.3	758.0 \pm 77.4	0.260 \pm 0.008	0.98* \pm 1.17	2.6* \pm 2.6	0.5 \pm 2.9	6.3 \pm 13.3	2.2 \pm 4.6	13.4* \pm 14.4	2.8* \pm 3.1
7		Yangtze Plain	33.3	1013.5 \pm 48.9	0.262 \pm 0.007	2.77* \pm 1.07	3.6* \pm 1.0	-0.8 \pm 1.8	7.4* \pm 8.3	2.1* \pm 2.4	29.2* \pm 6.9	4.4* \pm 1.0
8		Southeast China	24.2	1101.0 \pm 100.7	0.277 \pm 0.007	1.66* \pm 0.99	4.0* \pm 1.7	-1.2 \pm 2.4	7.5* \pm 9.0	2.9* \pm 3.5	36.6* \pm 12.9	4.3* \pm 1.5
9		Pearl	44.4	1026.5 \pm 73.4	0.240 \pm 0.007	2.10* \pm 1.04	0.3 \pm 1.4	-0.5 \pm 1.9	-3.2 \pm 12.2	-0.9 \pm 3.5	6.5 \pm 7.6	1.0 \pm 1.1
10		Hainan	41.3	953.8 \pm 103.2	0.225 \pm 0.009	1.50* \pm 1.52	2.9* \pm 2.0	1.7* \pm 3.3	5.6* \pm 6.6	4.2* \pm 5.0	21.9 \pm 14.4	2.7 \pm 1.8
11		Taiwan	12.8	2245.7 \pm 252.3	0.305 \pm 0.006	0.24 \pm 0.71	-0.5 \pm 3.1	-0.1 \pm 3.3	-2.1 \pm 9.3	-1.1 \pm 4.9	-9.4 \pm 60.7	-0.5 \pm 3.0
12	South Asia	East-Central India	24.8	336.1 \pm 35.5	0.166 \pm 0.003	1.40* \pm 0.66	12.9* \pm 4.1	5.5* \pm 5.6	17.2* \pm 10.8	29.9* \pm 18.7	26.1* \pm 5.4	9.4* \pm 1.9
13		Irrawaddy	29.8	746.0 \pm 81.5	0.214 \pm 0.006	2.83* \pm 1.15	10.8* \pm 2.3	4.2* \pm 3.2	35.2* \pm 12.8	18.5* \pm 6.7	45.5* \pm 8.8	8.2* \pm 1.6
14	Southeast Asia	Chao Phraya	27.8	734.0 \pm 76.8	0.208 \pm 0.006	0.88* \pm 1.24	3.2* \pm 1.9	1.8* \pm 2.6	8.7* \pm 11.1	4.2* \pm 5.4	14.9* \pm 8.3	2.8* \pm 1.6
15		Java-Bali	11.6	1069.9 \pm 103.5	0.227 \pm 0.009	0.46* \pm 1.53	0.6 \pm 1.8	1.3 \pm 4.4	1.8 \pm 4.6	2.0 \pm 5.0	4.1 \pm 15.5	0.4 \pm 1.6

Note: Bold and * indicates statistical significance ($p < .05$, paired Student's *t*-test); Italics indicates decrease.

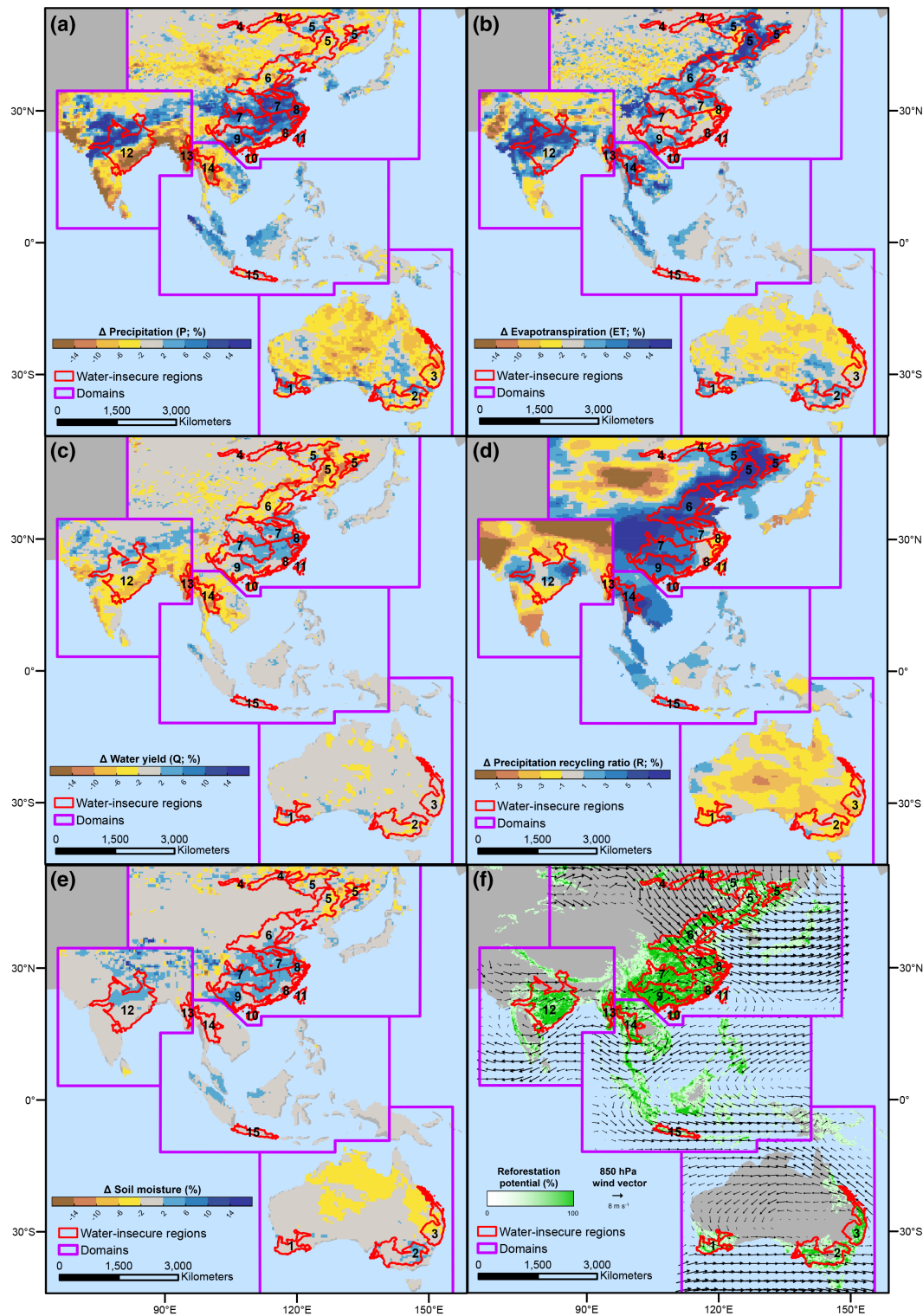


FIGURE 4 Mean percentage change in winter (DJF) precipitation (P) (a), evapotranspiration (ET) (b), water yield (Q) (c), the precipitation recycling ratio (R) (d), and soil moisture (e) between 2041 and 2070 in the Asia-Pacific, due to fully realizing the domain reforestation potential by 2040 (f). Baseline winter wind vectors at 850 hPa are shown in (f). Regional climate modeling was separately conducted for four CORDEX domains (Australasia, East Asia, South Asia, and Southeast Asia); domain boundaries indicated in this figure are the boundaries used for reporting results.

TABLE 4 Changes in summer (JJA) soil moisture (a), precipitation (P), local precipitation recycling ratio (R), and P from local and advected origin (b) compared with other key variables between 2041 and 2070 in water-insecure regions of the Asia-Pacific, due to fully realizing the domain reforestation potential by 2040. Figures reported are $M \pm SD$

No.	Domain	Region	(a) Summer (JJA) soil moisture			(b) Summer (JJA) precipitation recycling						
			Baseline mean % area reforestable	Baseline mean P (mm d^{-1})	Δ soil moisture (%)	ΔP (%)	ΔR (%)	Δ local P (mm yr^{-1})	$\% \Delta$ local P			
1	Australasia	Southwest Australia	19.0	0.79 ± 0.08	0.1222 ± 0.007	-1.4* ± 4.48	-1.8 ± 2.1	1.7 ± 16.8	0.00 ± 0.01	-0.7 ± 10.9	-0.01 ± 0.01	-1.9 ± 1.7
2		Murray-Darling	15.4	0.95 ± 0.19	0.1442 ± 0.012	0.31 ± 6.89	0.3 ± 4.4	1.3 ± 12.6	0.00 ± 0.01	3.1 ± 12.1	0.00 ± 0.03	0.0 ± 3.8
3		East Australia	26.5	0.61 ± 0.14	0.1117 ± 0.011	0.02 ± 7.49	1.9 ± 5.4	1.2 ± 10.6	0.00 ± 0.01	3.9 ± 14.3	0.01 ± 0.02	1.6 ± 4.1
4	East Asia	Siberia	16.4	2.87 ± 0.31	0.302 ± 0.016	-0.02 ± 3.97	0.5 ± 2.4	-0.7 ± 5.9	0.00 ± 0.07	-0.1 ± 5.4	0.01 ± 0.04	1.0 ± 2.6
5		Manchurian Plain	18.4	4.03 ± 0.29	0.303 ± 0.009	0.62 ± 2.39	0.1 ± 1.8	-0.3 ± 6.4	0.00 ± 0.08	0.2 ± 5.0	0.00 ± 0.04	0.1 ± 1.7
6		Loess Plateau–North China Plain	26.3	4.86 ± 0.48	0.286 ± 0.011	1.87* ± 2.89	4.2* ± 2.2	0.3 ± 5.6	0.09* ± 0.08	4.7* ± 4.3	0.11* ± 0.08	3.9* ± 2.7
7		Yangtze Plain	33.3	4.66 ± 0.35	0.272 ± 0.009	1.68* ± 2.63	0.7 ± 1.6	-0.4 ± 3.3	0.00 ± 0.07	0.2 ± 3.6	0.03 ± 0.03	1.1 ± 1.3
8		Southeast China	24.2	4.42 ± 0.48	0.292 ± 0.008	0.63 ± 2.13	1.3 ± 2.3	0.9 ± 5.3	0.03 ± 0.07	2.3 ± 5.0	0.03 ± 0.06	0.9 ± 1.9
9		Pearl	44.4	6.02 ± 0.58	0.294 ± 0.010	0.83 ± 2.73	-0.6 ± 2	-1.3 ± 3.8	-0.04 ± 0.1	-1.8 ± 4.2	0.00 ± 0.06	0.1 ± 1.7
10		Hainan	41.3	5.64 ± 0.69	0.295 ± 0.017	1.42 ± 4.75	2.3 ± 3.4	1.0 ± 6.5	0.02 ± 0.06	2.7 ± 6.5	0.1 ± 0.14	2.2 ± 2.9
11		Taiwan	12.8	10.73 ± 1.51	0.334 ± 0.006	0.08 ± 1.26	-1.3 ± 3.2	0.0 ± 8.9	-0.02 ± 0.08	-1.5 ± 6.9	-0.12 ± 0.24	-1.2 ± 2.6
12	South Asia	East-Central India	24.8	1.61 ± 0.37	0.170 ± 0.009	2.19* ± 4.06	16.9* ± 11.6	11.6* ± 16.7	0.11* ± 0.1	37.9* ± 34.1	0.16* ± 0.1	12.2* ± 7.2
13		Irrawaddy	29.8	5.54 ± 0.89	0.272 ± 0.027	8.16* ± 7.73	16.3* ± 3.4	6.2* ± 7.5	0.34* ± 0.13	24.1* ± 8.9	0.56* ± 0.12	13.6* ± 2.8
14	Southeast Asia	Chao Phraya	27.8	4.72 ± 0.64	0.269 ± 0.015	0.52 ± 4.52	2.8 ± 3.1	0.6 ± 7.3	0.04 ± 0.12	3.0 ± 9.2	0.09 ± 0.07	2.7 ± 2.0
15		Java-Bali	11.6	1.35 ± 0.28	0.191 ± 0.009	1.60* ± 4.17	5.6* ± 4.3	4.2* ± 10.7	0.01* ± 0.01	10.4* ± 11.9	0.07* ± 0.04	5.3* ± 3.3

Note: Bold and * indicates statistical significance ($p < 0.05$, paired student's t-test); italics indicates decrease.

TABLE 5 Changes in winter (DJF) soil moisture (a), precipitation (P), local precipitation recycling ratio (R), and P from local and advected origin (b) compared with other key variables between 2041 and 2070 in water-insecure regions of the Asia-Pacific, due to fully realizing the domain reforestation potential by 2040. Figures reported are $M \pm SD$

No.	Domain	Region	(a) Winter (DJF) soil moisture			(b) Winter (DJF) precipitation recycling			
			Baseline		Δ soil moisture (%)	ΔP (%)	ΔR (%)	Δ local P (mm yr^{-1})	% Δ local P
			% area reforestable	mean P (mm d^{-1})					
1	Australasia	Southwest Australia	19.0	0.48 ± 0.15	0.070 ± 0.003	0.24 ± 1.25	0.6 ± 4.4	-1.2 ± 9.1	0.00 ± 0.01
2		Murray-Darling	15.4	0.93 ± 0.23	0.084 ± 0.007	1.38 ± 2.00	0.2 ± 4.3	-1.3 ± 7.8	0.00 ± 0.01
3		East Australia	26.5	2.56 ± 0.46	0.129 ± 0.012	-1.69 ± 2.03	-4.8* ± 2.1	-1.6 ± 4.8	-0.04* ± 0.03
4	East Asia	Siberia	16.4	0.44 ± 0.05	0.222 ± 0.012	-1.17* ± 1.27	-1.4 ± 1.9	0.5 ± 5.5	0.00 ± 0.00
5		Manchurian Plain	18.4	0.6 ± 0.07	0.206 ± 0.010	-1.47* ± 1.10	-0.5 ± 1.3	6.3* ± 5.3	0.01* ± 0.00
6		Loess Plateau–North China Plain	26.3	0.24 ± 0.06	0.212 ± 0.008	0.85* ± 0.85	-0.3 ± 3.3	6.7* ± 5.3	0.00* ± 0.00
7		Yangtze Plain	33.3	1.01 ± 0.22	0.258 ± 0.010	3.43* ± 0.96	7.5* ± 3.8	4.3* ± 4.3	0.02* ± 0.01
8		Southeast China	24.2	1.34 ± 0.4	0.272 ± 0.012	2.07* ± 1.14	9* ± 3.5	-1.5 ± 5.4	0.01 ± 0.01
9		Pearl	44.4	0.78 ± 0.2	0.208 ± 0.009	2.95* ± 0.98	2.7 ± 3	4.3* ± 3.7	0.01* ± 0.01
10		Hainan	41.3	0.54 ± 0.17	0.173 ± 0.008	0.04 ± 1.47	-2.2 ± 9.6	2.3 ± 5.4	0.00 ± 0.00
11		Taiwan	12.8	2.11 ± 0.49	0.280 ± 0.009	0.93* ± 0.71	5.4* ± 2.7	-1.9 ± 4.4	0.00 ± 0.00
12	South Asia	East-Central India	24.8	0.58 ± 0.18	0.166 ± 0.006	1.05* ± 0.88	-7.4 ± 3.6	-1.9 ± 5.5	-0.01 ± 0.01
13		Irrawaddy	29.8	0.14 ± 0.07	0.167 ± 0.003	0.02 ± 0.67	-38.3* ± 10.7	-5.3* ± 2.9	-0.01* ± 0.00
14	Southeast Asia	Chao Phraya	27.8	0.16 ± 0.05	0.160 ± 0.003	0.51* ± 0.61	-8.6* ± 3.6	4.8* ± 3.9	0.00 ± 0.00
15		Java-Bali	11.6	4.61 ± 0.5	0.262 ± 0.013	0.22 ± 1.16	-0.2 ± 1.4	1.3 ± 7.6	0.01 ± 0.03

Note: Bold and * indicates statistical significance ($p < .05$, paired student's t-test); italics indicates decrease.

"disturbances" bringing some precipitation (Dimri et al., 2016), as indicated by the prevailing southwesterlies across the Deccan Plateau in central India (Figure 4f); north and central India thus benefit from increased precipitation (Figure 4a). However, the northeast winter monsoon carrying oceanic moisture to the eastern coast of India appears to weaken due to reforestation-induced land surface cooling reducing the land-sea thermal contrast (Figure S7). Overall, this combination of initial moisture limitation and favorable prevailing overland winds gives East-Central India the largest percentage increase in annual evapotranspiration ($10.9 \pm 6.2\%$) and precipitation ($12.9 \pm 4.1\%$) (both significant; Table 1) from reforestation out of all the water-insecure regions in the Asia-Pacific studied.

The East Asian summer monsoon also contains an inland component from prevailing winds traveling from southwest China (Pearl River basin and upper reaches of the Yangtze River basin) to the Loess Plateau–North China Plain (Figure 3f), which serve to propagate and recycle inland moisture from southwest up north. The Loess Plateau–North China Plain is the primary beneficiary in summer, with significant increases in local ($4.7 \pm 4.3\%$) and advected ($3.9 \pm 2.7\%$) precipitation and soil moisture ($1.9 \pm 2.9\%$) (Table 4). However, due to the weaker effects of the East Asian summer monsoon further north in the Manchurian Plain and Siberia, no significant increase in total, local, and advected summer precipitation is modeled there (Table 4). In winter, the Manchurian Plain and Siberia receive cold, dry continental winds from the Siberian High blowing out toward the Sea of Japan. Despite heightened winter evapotranspiration following reforestation, much of it is advected away, causing a decrease in total precipitation and hence soil moisture to be depleted (Figures 4a,b,e and Table 5a). Increased soil moisture in summer persists into the winter for the Loess Plateau–North China Plain, continuing to support a significant increase in locally generated precipitation ($6.0 \pm 5.3\%$), although total winter precipitation showed no significant change (Table 5). Some atmospheric moisture generated from the Loess Plateau–North China Plain is advected downwind to the Yangtze Plain and Southeast China (Figure 4a,b and Table 5), leading to a significant increase of $7.5 \pm 3.8\%$ and $9.0 \pm 3.5\%$ in total winter precipitation for those regions, respectively.

Overall, in our study, 7 of 15 regions had a significant increase in total annual precipitation, of which all also had a significant increase in advected precipitation, while six had a significant increase in local precipitation (Table 3b), pointing to the combined role of both increased local precipitation recycling as well as moisture transport from other reforested regions. Only 3 of 15 regions experienced nonsignificant declines in advected precipitation from reforestation. Our results provide the assurance that most water-insecure regions in the Asia-Pacific are unlikely to experience significant declines in advected precipitation following large-scale reforestation, with some regions significantly benefiting from advected moisture.

Although the evidence favors positive hydrological effects from reforestation, there are a number of water-insecure regions where a cautious approach to reforestation should be advisable (Table 1). Of the seven regions with nonsignificant declines in water yield, for three regions, this was due to heightened evapotranspiration

outstripping the increase in precipitation (Table 1), while for the remaining four regions, this was due to either a nonsignificant decline in soil moisture (Table 3), advected precipitation (Table 3b), or both. Only one region showed a significant decline in precipitation (East Australia, $-2.0 \pm 2.2\%$)—this region also showed nonsignificant declines in soil moisture, local precipitation, and advected precipitation.

5 | DISCUSSION AND CONCLUSION

Our simulations use a five-model ensemble to show that even a more realistic and modest reforestation scenario can deliver significant hydrological benefits for many water-insecure regions, which will be directly relevant to contemporary reforestation policies. We found that the divergent responses of precipitation to reforestation can be explained by the degree of initial moisture limitation, and existing large-scale circulation patterns driving atmospheric moisture transport, especially in monsoon regions. Similar to studies using realistic reforestation scenarios, we did not observe large changes to basic monsoon patterns (Li et al., 2018).

There are well-founded concerns that forestation projects in water-stressed or semiarid regions may ultimately reduce water yield (Trimble et al., 1987; Yao et al., 2015). Much of these concerns have stemmed from the experience of revegetation in north China (including the Loess Plateau) over the past decades, which was suggested to increase evapotranspiration without any significant increase in precipitation to compensate (Feng et al., 2016), although models and observations have suggested contradictory results for precipitation feedback (Cao et al., 2019; Ge et al., 2020; Lv et al., 2019; Zhang et al., 2022). Different reasons have been suggested, such as the newly planted vegetation not having sufficient time yet to mature into forest (Ge et al., 2020), suppressed precipitation over north China due to anthropogenic aerosols (Duan & Mao, 2008; Li et al., 2018), or the overlooked role of vegetation-climate feedbacks (Zhang et al., 2022). Our study uses RCP4.5 forcings from five models for 2040–2070, with reforested lands becoming forest cover by 2040, and so cannot be directly compared to observations, models forced with observations, and different reforestation scenarios. However, our results appear to suggest that the Loess Plateau–North China Plain can benefit from advected moisture from reforestation in southwest China and the Yangtze Plain in summer, with some of the positive hydrological effects persisting through winter even as some moisture is advected away. We also found that the lack of precipitation increase in some regions from reforestation (e.g., Manchurian Plain) is likely due to moisture being advected away. As such, future studies on reforestation and hydrology could benefit from considering atmospheric moisture transport.

Our study suggests that while some water-insecure regions can benefit hydrologically from large-scale reforestation, a more cautious approach would continue to be advisable for some water-insecure regions with equivocal results (Table 1). Nevertheless, despite the positive results from our regional-scale modeling,

reforestation projects still require careful consideration of local environmental conditions, with scientifically sound management and species selection, to avoid negative environmental consequences (Cao et al., 2010, 2011). Although we used a five-model RegCM ensemble to generate our results, with each model generally performing well in reproducing climatic patterns at 40-km resolution, smaller spatial scales may require models such as the Weather Research and Forecasting (WRF) model which can improve representation of finer scale processes (Hong et al., 2015; Vu et al., 2016). Finally, the possibility that reforestation can help to modulate climatic extremes has also been suggested (Belušić et al., 2019; Locatelli et al., 2015). We provide evidence that reforestation could reduce drought risk for many water-insecure regions, and thus be a useful tool for holistic water management for climate adaptation alongside other methods (Grobicki et al., 2015; He et al., 2019, 2021; Teo, Hill, et al., 2021; Wan et al., 2018).

Overall, our results show that reforestation can lead to positive hydrological effects for many water-insecure regions in the Asia-Pacific, such as increases in water yield, precipitation, soil moisture, and reductions in drought risk. Reforestation was assessed to be hydrologically beneficial to water yield in 7 of 15 water-insecure regions with medium to high confidence (Table 1). These water-insecure regions are home to 928 million people, of 1.3 billion people living in water-insecure regions across the Asia-Pacific in 2020 (WorldPop, 2021) (Table S2). Of the 15 water-insecure regions in the Asia-Pacific, 14 cross a domestic state or provincial boundary, while five are transnational, highlighting the need for transboundary cooperation and policies (Lechner et al., 2020; Narain et al., 2020; Teo et al., 2020). There is therefore considerable potential for further research and application of reforestation as a transboundary nature-based solution for enhancing the water-energy-food nexus (Leck et al., 2015; Sreekar et al., 2022; Taniguchi et al., 2017; Zheng et al., 2022), especially in support of the United Nations Decade on Ecosystem Restoration, and pledges by 141 countries to restore ecosystems at the 26th United Nations Climate Change Conference in 2021 (COP26) (United Nations, 2021).

AUTHOR CONTRIBUTIONS

Hoong Chen Teo, Lian Pin Koh, Srivatsan V. Raghavan, and Xiaogang He conceived the study. Lian Pin Koh supervised the study. Hoong Chen Teo, Lian Pin Koh, Srivatsan V. Raghavan, and Xiaogang He, Zhenzhong Zeng, Yanyan Cheng, and Xiangzhong Luo contributed to designing the methodologies. Hoong Chen Teo conducted the analyses and led the writing. All authors contributed to writing and editing.

ACKNOWLEDGMENTS

L.P.K. is supported by the Singapore National Research Foundation (NRF-RSS2019-007). X.H. is supported by the Singapore Ministry of Education Academic Research Fund Tier-1 projects (A-0009297-01-00 and A-8000190-00-00). X.L. is supported by the Singapore Ministry of Education (R-109-000-272-133).

CONFLICT OF INTEREST

The authors declare no competing interests.

DATA AVAILABILITY STATEMENT

All data are available in the main text or the supplementary materials. Raw data and spatial data are available at <https://doi.org/10.5061/dryad.5mkwh78k>.

ORCID

- Hoong Chen Teo  <https://orcid.org/0000-0003-0127-978X>
- Srivatsan V. Raghavan  <https://orcid.org/0000-0002-8008-0295>
- Xiaogang He  <https://orcid.org/0000-0001-7428-0269>
- Zhenzhong Zeng  <https://orcid.org/0000-0001-6851-2756>
- Yanyan Cheng  <https://orcid.org/0000-0002-2065-6512>
- Xiangzhong Luo  <https://orcid.org/0000-0002-9546-0960>
- Alex M. Lechner  <https://orcid.org/0000-0003-2050-9480>
- Matthew J. Ashfold  <https://orcid.org/0000-0002-2191-1554>
- Aakash Lamba  <https://orcid.org/0000-0002-5060-4350>
- Rachakonda Sreekar  <https://orcid.org/0000-0001-5445-6589>
- Qiming Zheng  <https://orcid.org/0000-0002-7393-6585>
- Anping Chen  <https://orcid.org/0000-0003-2085-3863>
- Lian Pin Koh  <https://orcid.org/0000-0001-8152-3871>

REFERENCES

- Abiodun, B. J., Adeyewa, Z. D., Oguntunde, P. G., Salami, A. T., & Ajayi, V. O. (2012). Modeling the impacts of reforestation on future climate in West Africa. *Theoretical and Applied Climatology*, 110(1-2), 77–96. <https://doi.org/10.1007/s00704-012-0614-1>
- Alkon, M., He, X., Paris, A. R., Liao, W., Hodson, T., Wanders, N., & Wang, Y. (2019). Water security implications of coal-fired power plants financed through China's belt and road initiative. *Energy Policy*, 132, 1101–1109. <https://doi.org/10.1016/J.ENPOL.2019.06.044>
- Bader, B., & Yan, J. (2020). Package 'eva': Extreme value analysis with goodness-of-fit testing. R Package Version 0.2.6. <https://cran.r-project.org/web/packages/eva/eva.pdf>
- Bader, B., Yan, J., & Zhang, X. (2016). Automated selection of r for the r largest order statistics approach with adjustment for sequential testing. *Statistics and Computing*, 27(6), 1435–1451. <https://doi.org/10.1007/S11222-016-9697-3>
- Belušić, D., Fuentes-Franco, R., Strandberg, G., & Jukimenko, A. (2019). Afforestation reduces cyclone intensity and precipitation extremes over Europe. *Environmental Research Letters*, 14(7), 074009. <https://doi.org/10.1088/1748-9326/AB23B2>
- Bennett, B. M., & Barton, G. A. (2018). The enduring link between forest cover and rainfall: A historical perspective on science and policy discussions. *Forest Ecosystems*, 5(1), 1–9. <https://doi.org/10.1186/S40663-017-0124-9>
- Brubaker, K. L., Entekhabi, D., & Eagleson, P. S. (1993). Estimation of continental precipitation recycling. *Journal of Climate*, 6(6), 1077–1089. [https://doi.org/10.1175/1520-0442\(1993\)006<1077:EOCP>2.0.CO;2](https://doi.org/10.1175/1520-0442(1993)006<1077:EOCP>2.0.CO;2)
- Cai, J., Liu, Y., Lei, T., & Pereira, L. S. (2007). Estimating reference evapotranspiration with the FAO penman-Monteith equation using daily weather forecast messages. *Agricultural and Forest Meteorology*, 145(1-2), 22–35. <https://doi.org/10.1016/J.AGRFORMAT.2007.04.012>
- Cao, Q., Wu, J., Yu, D., & Wang, W. (2019). The biophysical effects of the vegetation restoration program on regional climate metrics in the

- loess plateau, China. *Agricultural and Forest Meteorology*, 268, 169–180. <https://doi.org/10.1016/J.AGRIFORMET.2019.01.022>
- Cao, S., Chen, L., Shankman, D., Wang, C., Wang, X., & Zhang, H. (2011). Excessive reliance on afforestation in China's arid and semi-arid regions: Lessons in ecological restoration. *Earth-Science Reviews*, 104(4), 240–245. <https://doi.org/10.1016/J.EARSCIREV.2010.11.002>
- Cao, S., Tian, T., Chen, L., Dong, X., Yu, X., & Wang, G. (2010). Damage caused to the environment by reforestation policies in arid and semi-arid areas of China. *Ambio*, 39, 279–283. <https://doi.org/10.1007/s13280-010-0038-z>
- Cerasoli, S., Yin, J., & Porporato, A. (2021). Cloud cooling effects of afforestation and reforestation at midlatitudes. *Proceedings of the National Academy of Sciences*, 118(33), e2026241118. <https://doi.org/10.1073/PNAS.2026241118>
- Chen, M., Vernon, C. R., Graham, N. T., Hejazi, M., Huang, M., Cheng, Y., & Calvin, K. (2020). Global land use for 2015–2100 at 0.05° resolution under diverse socioeconomic and climate scenarios. *Scientific Data*, 7, 320. <https://doi.org/10.1038/s41597-020-00669-x>
- Cheng, Y., Huang, M., Lawrence, D. M., Calvin, K., Lombardozzi, D. L., Sinha, E., Pan, M., & He, X. (2022). Future bioenergy expansion could alter carbon sequestration potential and exacerbate water stress in the United States. *Science Advances*, 8(18), 8237. https://doi.org/10.1126/SCIAADV.ABM8237/SUPPL_FILE/SCIAADV.ABM8237_SM.PDF
- Cheng, Y., Leung, L. R., Huang, M., Koven, C., Detto, M., Knox, R., Bisht, G., Bretfeld, M., & Fisher, R. A. (2022). Modeling the joint effects of vegetation characteristics and soil properties on ecosystem dynamics in a Panama tropical Forest. *Journal of Advances in Modeling Earth Systems*, 14(1), e2021MS002603. <https://doi.org/10.1029/2021MS002603>
- Cheng, Y., Ogden, F. L., Zhu, J., & Bretfeld, M. (2018). Land use-dependent preferential flow paths affect hydrological response of steep tropical lowland catchments with Saprolitic soils. *Water Resources Research*, 54(8), 5551–5566. <https://doi.org/10.1029/2017WR021875>
- Cui, M., Ferreira, F., Fung, T. K., & Matos, J. S. (2021). Tale of two cities: How nature-based solutions help create adaptive and resilient urban water management practices in Singapore and Lisbon. *Sustainability*, 13(18), 10427. <https://doi.org/10.3390/SU131810427>
- Dimri, A. P., Yasunari, T., Kotlia, B. S., Mohanty, U. C., & Sikka, D. R. (2016). Indian winter monsoon: Present and past. *Earth-Science Reviews*, 163, 297–322. <https://doi.org/10.1016/J.EARSCIREV.2016.10.008>
- Duan, J., & Mao, J. (2008). Influence of aerosol on regional precipitation in North China. *Chinese Science Bulletin*, 54(3), 474–483. <https://doi.org/10.1007/S11434-008-0447-6>
- Ellison, D., Futter, M. N., & Bishop, K. (2012). On the forest cover-water yield debate: From demand- to supply-side thinking. *Global Change Biology*, 18(3), 806–820. <https://doi.org/10.1111/j.1365-2486.2011.02589.x>
- Emanuel, K. A. (1991). A scheme for representing cumulus convection in large-scale models. *Journal of the Atmospheric Sciences*, 48(21), 2313–2329. [https://doi.org/10.1175/1520-0469\(1991\)048<2313:ASFRC>2.0.CO;2](https://doi.org/10.1175/1520-0469(1991)048<2313:ASFRC>2.0.CO;2)
- Fargione, J., Hill, J., Tilman, D., Polasky, S., & Hawthorne, P. (2008). Land clearing and the biofuel carbon debt. *Science*, 319(5867), 1235–1238. <https://doi.org/10.1126/SCIENCE.1152747>
- Feng, X., Fu, B., Piao, S., Wang, S., Ciais, P., Zeng, Z., Lü, Y., Zeng, Y., Li, Y., Jiang, X., & Wu, B. (2016). Revegetation in China's loess plateau is approaching sustainable water resource limits. *Nature Climate Change*, 6(11), 1019–1022. <https://doi.org/10.1038/nclimate3092>
- Filos, S., Bezerra, M. O., Weiss, K. C. B., & Palmer, M. A. (2017). Impacts of forest restoration on water yield: A systematic review. *PLoS One*, 12(8), e0183210. <https://doi.org/10.1371/JOURNALALPONE.0183210>
- Ge, J., Pitman, A. J., Guo, W., Zan, B., & Fu, C. (2020). Impact of revegetation of the loess plateau of China on the regional growing season water balance. *Hydrology and Earth System Sciences*, 24(2), 515–533. <https://doi.org/10.5194/HESS-24-515-2020>
- Griscom, B. W., Adams, J., Ellis, P. W., Houghton, R. A., Lomax, G., Miteva, D. A., Schlesinger, W. H., Shoch, D., Siikamäki, J. V., Smith, P., Woodbury, P., Zganjar, C., Blackman, A., Campari, J., Conant, R. T., Delgado, C., Elias, P., Gopalakrishna, T., Hamsik, M. R., ... Fargione, J. (2017). Natural climate solutions. *Proceedings of the National Academy of Sciences of the United States of America*, 114(44), 11645–11650. <https://doi.org/10.1073/pnas.1710465114>
- Grobicki, A., MacLeod, F., & Pischke, F. (2015). Integrated policies and practices for flood and drought risk management. *Water Policy*, 17(S1), 180–194. <https://doi.org/10.2166/WP.2015.009>
- Gupta, S. K., Deshpande, R. D., Bhattacharya, S. K., & Jani, R. A. (2005). Groundwater $\delta^{18}\text{O}$ and δD from central Indian Peninsula: Influence of the Arabian Sea and the bay of Bengal branches of the summer monsoon. *Journal of Hydrology*, 303(1–4), 38–55. <https://doi.org/10.1016/J.JHYDROL.2004.08.016>
- Hamon, W. R. (1961). Estimating potential evapotranspiration. *Journal of the Hydraulics Division*, 87(3), 107–120. <https://doi.org/10.1061/JYCEAJ.0000599>
- He, X., Bryant, B. P., Moran, T., Mach, K. J., Wei, Z., & Freyberg, D. L. (2021). Climate-informed hydrologic modeling and policy typology to guide managed aquifer recharge. *Science Advances*, 7(17), 6025–6046. https://doi.org/10.1126/SCIAADV.ABE6025/SUPPL_FILE/ABE6025_SM.PDF
- He, X., Estes, L., Konar, M., Tian, D., Anghileri, D., Baylis, K., Evans, T. P., & Sheffield, J. (2019). Integrated approaches to understanding and reducing drought impact on food security across scales. *Current Opinion in Environmental Sustainability*, 40, 43–54. <https://doi.org/10.1016/J.COSUST.2019.09.006>
- Hersbach, H., Bell, B., Berrisford, P., Biavati, G., Horányi, A., Muñoz Sabater, J., Nicolas, J., Peubey, C., Radu, R., Rozum, I., Schepers, D., Simmons, A., Soci, C., Dee, D., & Thépaut, J.-N. (2019). ERA5 monthly averaged data on single levels from 1979 to present. Copernicus Climate Change Service (C3S) Climate Data Store (CDS) <https://doi.org/10.24381/cds.f17050d7>
- Hoek van Dijke, A. J., Herold, M., Mallick, K., Benedict, I., Machwitz, M., Schlerf, M., Pranindita, A., Theeuwen, J. J. E., Bastin, J.-F., & Teuling, A. J. (2022). Shifts in regional water availability due to global tree restoration. *Nature Geoscience*, 15(5), 363–368. <https://doi.org/10.1038/s41561-022-00935-0>
- Holgate, C. M., Evans, J. P., van Dijk, A. I. J. M., Pitman, A. J., & Di Virgilio, G. (2020). Australian precipitation recycling and evaporative source regions. *Journal of Climate*, 33(20), 8721–8735. <https://doi.org/10.1175/JCLI-D-19-0926.1>
- Holtslag, A. A. M., De Bruijn, E. I. F., & Pan, H.-L. (1990). A high resolution air mass transformation model for short-range weather forecasting. *Monthly Weather Review*, 118(8), 1561–1575. [https://doi.org/10.1175/1520-0493\(1990\)118<1561:AHRAMT>2.0.CO;2](https://doi.org/10.1175/1520-0493(1990)118<1561:AHRAMT>2.0.CO;2)
- Hong, Y., He, X., Cerato, A., Zhang, K., Hong, Z., & Liao, Z. (2015). Predictability of a physically based model for rainfall-induced shallow landslides: Model development and case studies. In M. Scaioni (Ed.), *Modern technologies for landslide monitoring and prediction*. Springer Natural Hazards (pp. 165–178). Springer. https://doi.org/10.1007/978-3-662-45931-7_9
- Hurtl, G. C., Chini, L. P., Frolking, S., Betts, R. A., Feddema, J., Fischer, G., Fisk, J. P., Hibbard, K., Houghton, R. A., Janetos, A., Jones, C. D., Kindermann, G., Kinoshita, T., Klein Goldewijk, K., Riahi, K., Sheviakova, E., Smith, S., Stehfest, E., Thomson, A., ... Wang, Y. P. (2011). Harmonization of land-use scenarios for the period 1500–2100: 600 years of global gridded annual land-use transitions,

- wood harvest, and resulting secondary lands. *Climatic Change*, 109(1), 117–161. <https://doi.org/10.1007/s10584-011-0153-2>
- Karadan, M. M., Raju, P. V. S., & Mishra, A. (2021). Simulations of Indian summer monsoon using RegCM: A comparison with ERA and GFDL analysis. *Theoretical and Applied Climatology*, 143(3), 1381–1391. <https://doi.org/10.1007/S00704-020-03496-7>
- Kemppinen, K. M. S., Collins, P. M., Hole, D. G., Wolf, C., Ripple, W. J., & Gerber, L. R. (2020). Global reforestation and biodiversity conservation. *Conservation Biology*, 34(5), 1221–1228. <https://doi.org/10.1111/COBI.13478>
- Koh, L. P., Zeng, Y., Sarira, T. V., & Siman, K. (2021). Carbon prospecting in tropical forests for climate change mitigation. *Nature Communications*, 12(1), 1–9. <https://doi.org/10.1038/s41467-021-21560-2>
- Koster, R. D., Dirmeyer, P. A., Guo, Z., Bonan, G., Chan, E., Cox, P., Gordon, C. T., Kanae, S., Kowalczyk, E., Lawrence, D., Liu, P., Lu, C. H., Malyshev, S., McAvaney, B., Mitchell, K., Mocko, D., Oki, T., Oleson, K., Pitman, A., ... Yamada, T. (2004). Regions of strong coupling between soil moisture and precipitation. *Science*, 305(5687), 1138–1140. <https://doi.org/10.1126/SCIENCE.1100217>
- Koster, R. D., Suarez, M. J., Higgins, R. W., & Van den Dool, H. M. (2003). Observational evidence that soil moisture variations affect precipitation. *Geophysical Research Letters*, 30(5), 1241. <https://doi.org/10.1029/2002GL016571>
- Kumar, D., & Dimri, A. P. (2020). Sensitivity of convective and land surface parameterization in the simulation of contrasting monsoons over CORDEX-South Asia domain using RegCM-4.4.5.5. *Theoretical and Applied Climatology*, 139(1–2), 297–322. <https://doi.org/10.1007/S00704-019-02976-9/FIGURES/14>
- Lawrence, D. M., Thornton, P. E., Oleson, K. W., & Bonan, G. B. (2007). The partitioning of evapotranspiration into transpiration, soil evaporation, and canopy evaporation in a GCM: Impacts on land-atmosphere interaction. *Journal of Hydrometeorology*, 8(4), 862–880. <https://doi.org/10.1175/JHM596.1>
- Lechner, A. M., Gomes, R. L., Rodrigues, L., Ashfold, M. J., Selvam, S. B., Wong, E. P., Raymond, C. M., Zieritz, A., Sing, K. W., Moug, P., Billia, L., Sagala, S., Cheshmehzangi, A., Lourdes, K., Azhar, B., Sanusi, R., Ives, C. D., Tang, Y.-T., Tan, D. T., ... Gibbins, C. (2020). Challenges and considerations of applying nature-based solutions in low- and middle-income countries in southeast and East Asia. *Blue-Green Systems*, 2, 331–351. <https://doi.org/10.2166/bgs.2020.014>
- Leck, H., Conway, D., Bradshaw, M., & Rees, J. (2015). Tracing the water-energy-food nexus: Description theory and practice. *Geography Compass*, 9(8), 445–460. <https://doi.org/10.1111/GEC3.12222>
- Lehner, B., & Grill, G. (2013). Global river hydrography and network routing: Baseline data and new approaches to study the world's large river systems. *Hydrological Processes*, 27(15), 2171–2186. <https://doi.org/10.1002/HYP.9740>
- Li, Y., Piao, S., Li, L. Z. X., Chen, A., Wang, X., Ciais, P., Huang, L., Lian, X., Peng, S., Zeng, Z., Wang, K., & Zhou, L. (2018). Divergent hydrological response to large-scale afforestation and vegetation greening in China. *Science Advances*, 4(5), eaar4182. <https://doi.org/10.1126/SCIAADV.AAR4182>
- Locatelli, B., Catterall, C. P., Imbach, P., Kumar, C., Lasco, R., Marín-Spiotta, E., Mercer, B., Powers, J. S., Schwartz, N., & Uriarte, M. (2015). Tropical reforestation and climate change: Beyond carbon. *Restoration Ecology*, 23(4), 337–343. <https://doi.org/10.1111/REC.12209>
- Lu, J., Sun, G., McNulty, S. G., & Amatya, D. M. (2005). A comparison of six potential evapotranspiration methods for regional use in the southeastern United States. *Journal of the American Water Resources Association*, 41(3), 621–633. <https://doi.org/10.1111/J.1752-1688.2005.TB03759.X>
- Luck, M., Landis, M., & Gassert, F. (2015). Aqueduct water stress projections: Decadal projections of water supply and demand using CMIP5 GCMs. <https://www.wri.org/publication/aqueduct-water-stress-projections-decadal-projections-water-supply-and-demand-using>
- Lv, M., Ma, Z., & Peng, S. (2019). Responses of terrestrial water cycle components to afforestation within and around the Yellow River basin. *Atmospheric and Oceanic Science Letters*, 12(2), 116–123. <https://doi.org/10.1080/16742834.2019.1569456>
- Maity, S., Nayak, S., Singh, K. S., Nayak, H. P., & Dutta, S. (2021). Impact of soil moisture initialization in the simulation of Indian summer monsoon using RegCM4. *Atmosphere*, 12(9), 1148. <https://doi.org/10.3390/ATMOS12091148>
- Meier, R., Schwaab, J., Seneviratne, S. I., Sprenger, M., Lewis, E., & Davin, E. L. (2021). Empirical estimate of forestation-induced precipitation changes in Europe. *Nature Geoscience*, 14(7), 473–478. <https://doi.org/10.1038/s41561-021-00773-6>
- Mori, A. S., Dee, L. E., Gonzalez, A., Ohashi, H., Cowles, J., Wright, A. J., Loreau, M., Hautier, Y., Newbold, T., Reich, P. B., Matsui, T., Takeuchi, W., Okada, K., Seidl, R., & Isbell, F. (2021). Biodiversity–productivity relationships are key to nature-based climate solutions. *Nature Climate Change*, 11(6), 543–550. <https://doi.org/10.1038/s41558-021-01062-1>
- Narain, D., Maron, M., Teo, H. C., Hussey, K., & Lechner, A. M. (2020). Best-practice biodiversity safeguards for belt and road Initiative's financiers. *Nature Sustainability*, 3, 650–657. <https://doi.org/10.1038/s41893-020-0528-3>
- Navarro-Racines, C., Tarapues, J., Thornton, P., Jarvis, A., & Ramirez-Villegas, J. (2020). High-resolution and bias-corrected CMIP5 projections for climate change impact assessments. *Scientific Data*, 7, 7. <https://doi.org/10.1038/s41597-019-0343-8>
- Oleson, K., Lawrence, D. M., Bonan, G. B., Drewniak, B., Huang, M., Koven, C. D., Levis, S., Li, F., Riley, W. J., Subin, Z. M., Swenson, S., Thornton, P. E., Bozbiyik, A., Fisher, R., Heald, C. L., Kluzek, E., Lamarque, J.-F., Lawrence, P. J., Leung, L. R., ... Yang, Z.-L. (2013). Technical description of version 4.5 of the Community Land Model (CLM). (No. NCAR/TN-503+STR). <https://doi.org/10.5065/D6RR1W7M>
- Pal, J. S., Small, E. E., & Eltahir, E. A. B. (2000). Simulation of regional-scale water and energy budgets: Representation of subgrid cloud and precipitation processes within RegCM. *Journal of Geophysical Research: Atmospheres*, 105(D24), 29579–29594. <https://doi.org/10.1029/2000JD900415>
- Paparrizos, S., Maris, F., & Matzarakis, A. (2016). Sensitivity analysis and comparison of various potential evapotranspiration formulae for selected Greek areas with different climate conditions. *Theoretical and Applied Climatology*, 128(3), 745–759. <https://doi.org/10.1007/S00704-015-1728-Z>
- Pathak, A., Ghosh, S., & Kumar, P. (2014). Precipitation recycling in the Indian subcontinent during summer monsoon. *Journal of Hydrometeorology*, 15(5), 2050–2066. <https://doi.org/10.1175/JHM-D-13-0172.1>
- Sarira, T. V., Zeng, Y., Neugarten, R., Chaplin-Kramer, R., & Koh, L. P. (2022). Co-benefits of forest carbon projects in Southeast Asia. *Nature Sustainability*, 5(5), 393–396. <https://doi.org/10.1038/s41893-022-00849-0>
- Satoh, Y., Kahil, T., Byers, E., Burek, P., Fischer, G., Tramberend, S., Greve, P., Flörke, M., Eisner, S., Hanasaki, N., Magnuszewski, P., Nava, L. F., Cosgrove, W., Langan, S., & Wada, Y. (2017). Multi-model and multi-scenario assessments of Asian water futures: The water futures and solutions (WFaS) initiative. *Earth's Future*, 5(7), 823–852. <https://doi.org/10.1002/2016EF000503>
- Schymanski, S. J., & Or, D. (2017). Leaf-scale experiments reveal an important omission in the Penman-Monteith equation. *Hydrology and Earth System Sciences*, 21(2), 685–706. <https://doi.org/10.5194/HESS-21-685-2017>
- Sellers, P. J., Randall, D. A., Collatz, G. J., Berry, J. A., Field, C. B., Dazlich, D. A., Zhang, C., Collelo, G. D., & Bounoua, L. (1996). A revised

- land surface parameterization (SiB2) for atmospheric GCMS. Part I: Model formulation. *Journal of Climate*, 9(4), 676–705. [https://doi.org/10.1175/1520-0442\(1996\)009<0676:ARLSPF>2.0.CO;2](https://doi.org/10.1175/1520-0442(1996)009<0676:ARLSPF>2.0.CO;2)
- Seneviratne, S. I., Corti, T., Davin, E. L., Hirschi, M., Jaeger, E. B., Lehner, I., Orlowsky, B., & Teuling, A. J. (2010). Investigating soil moisture-climate interactions in a changing climate: A review. *Earth-Science Reviews*, 99(3–4), 125–161. <https://doi.org/10.1016/J.EARSCIREV.2010.02.004>
- Sengupta, S., & Sarkar, A. (2006). Stable isotope evidence of dual (Arabian Sea and Bay of Bengal) vapour sources in monsoonal precipitation over North India. *Earth and Planetary Science Letters*, 250(3–4), 511–521. <https://doi.org/10.1016/J.EPSL.2006.08.011>
- Sreekar, R., Zeng, Y., Zheng, Q., Lamba, A., Teo, H. C., Sarira, T. V., & Koh, L. P. (2022). Nature-based climate solutions for expanding the global protected area network. *Biological Conservation*, 269, 109529. <https://doi.org/10.1016/J.BIOCON.2022.109529>
- Taniguchi, M., Endo, A., Gurdak, J. J., & Swarzenski, P. (2017). Water-energy-food nexus in the Asia-Pacific region. *Journal of Hydrology: Regional Studies*, 11, 1–8. <https://doi.org/10.1016/J.EJRH.2017.06.004>
- Teo, H. C., Campos-Arceiz, A., Li, B. V., Wu, M., & Lechner, A. M. (2020). Building a green belt and road: A systematic review and comparative assessment of the Chinese and English-language literature. *PLoS One*, 15(9), e0239009. <https://doi.org/10.1371/journal.pone.0239009>
- Teo, H. C., Hill, M. J., Lechner, A. M., Teo, F. Y., & Gibbins, C. N. (2021). Landscape-scale remote sensing and classification of lentic habitats in a tropical city. *Wetlands*, 41(7), 1–15. <https://doi.org/10.1007/S13157-021-01491-W>
- Teo, H. C., Zeng, Y., Sarira, T. V., Fung, T. K., Zheng, Q., Song, X. P., Chong, K. Y., & Koh, L. P. (2021). Global urban reforestation can be an important natural climate solution. *Environmental Research Letters*, 16(3), 034059. <https://doi.org/10.1088/1748-9326/abe783>
- Trimble, S. W., Weirich, F. H., & Hoag, B. L. (1987). Reforestation and the reduction of water yield on the southern Piedmont since circa 1940. *Water Resources Research*, 23(3), 425–437. <https://doi.org/10.1029/WR023I003P00425>
- United Nations. (2021). *Glasgow leaders' declaration on forests and land use*. UN Climate Change Conference, UK 2021. <https://ukcop26.org/glasgow-leaders-declaration-on-forests-and-land-use/>
- Vu, M. T., Raghavan, V. S., & Lioung, S. Y. (2016). Deriving short-duration rainfall IDF curves from a regional climate model. *Natural Hazards*, 85(3), 1877–1891. <https://doi.org/10.1007/S11069-016-2670-9>
- Wan, W., Zhao, J., Li, H. Y., Mishra, A., Hejazi, M., Lu, H., Demissie, Y., & Wang, H. (2018). A holistic view of water management impacts on future droughts: A global multimodel analysis. *Journal of Geophysical Research: Atmospheres*, 123(11), 5947–5972. <https://doi.org/10.1029/2017JD027825>
- Wang, L., Good, S. P., & Caylor, K. K. (2014). Global synthesis of vegetation control on evapotranspiration partitioning. *Geophysical Research Letters*, 41(19), 6753–6757. <https://doi.org/10.1002/2014GL061439>
- WorldPop. (2021). *Earth engine data catalog*. https://developers.google.com/earth-engine/datasets/catalog/WorldPop_GP_100m_pop
- Yao, Y., Cai, T., Ju, C., & He, C. (2015). Effect of reforestation on annual water yield in a large watershed in Northeast China. *Journal of Forestry Research*, 26(3), 697–702. <https://doi.org/10.1007/s11676-015-0119-8>
- Zeng, X., Zhao, M., & Dickinson, R. E. (1998). Intercomparison of bulk aerodynamic algorithms for the computation of sea surface fluxes using TOGA COARE and TAO data. *Journal of Climate*, 11(10), 2628–2644. [https://doi.org/10.1175/1520-0442\(1998\)011<2628:IOBA>2.0.CO;2](https://doi.org/10.1175/1520-0442(1998)011<2628:IOBA>2.0.CO;2)
- Zhang, B., Tian, L., Yang, Y., & He, X. (2022). Revegetation does not decrease water yield in the loess plateau of China. *Geophysical Research Letters*, 49(9), e2022GL098025. <https://doi.org/10.1029/2022GL098025>
- Zhang, L., Dawes, W. R., & Walker, G. R. (2001). Response of mean annual evapotranspiration to vegetation changes at catchment scale. *Water Resources Research*, 37(3), 701–708. <https://doi.org/10.1029/2000WR900325>
- Zheng, Q., Siman, K., Zeng, Y., Teo, H. C., Sarira, T. V., Sreekar, R., & Koh, L. P. (2022). Future land-use competition constrains natural climate solutions. *Science of the Total Environment*, 838, 156409. <https://doi.org/10.1016/J.SCITOTENV.2022.156409>

SUPPORTING INFORMATION

Additional supporting information can be found online in the Supporting Information section at the end of this article.

How to cite this article: Teo, H. C., Raghavan, S. V., He, X., Zeng, Z., Cheng, Y., Luo, X., Lechner, A. M., Ashfold, M. J., Lamba, A., Sreekar, R., Zheng, Q., Chen, A., & Koh, L. P. (2022). Large-scale reforestation can increase water yield and reduce drought risk for water-insecure regions in the Asia-Pacific. *Global Change Biology*, 00, 1–19. <https://doi.org/10.1111/gcb.16404>